

# Hybrid CFD/BEM Approach to Predict Flow Induced Noise

**P. Croaker (1), R. Kinns (1), N. Kessissoglou (1),  
D. Norrison (2), R. Widjaja (2), S. Marburg (3)**

(1) School of Mechanical and Manufacturing Engineering, The University of New South Wales, Sydney, Australia

(2) Maritime Platforms Division, Defence Science and Technology Organisation, Melbourne, Australia

(3) Institute of Mechanics, Universität der Bundeswehr München, Neubiberg, Germany

**PACS:** 43.28 Ra

## ABSTRACT

A computational approach is proposed to extract the acoustic sources generated by low Mach number flow past a circular cylinder and to predict the associated far-field acoustic pressure. The transient hydrodynamic flow field is calculated using an incompressible computational fluid dynamics (CFD) solver. The acoustic sources are extracted from the hydrodynamic flow field based on the linearised perturbed compressible equations (LPCE). These acoustic sources are combined with a boundary element method (BEM) model of a rigid circular cylinder and the far field sound pressure level is predicted. The results from this hybrid CFD/BEM approach are presented for flow past a circular cylinder with Reynolds number,  $Re_D=100$  and Mach number,  $M=0.15$ . The directivity of the radiated sound pressure field at the vortex shedding frequency agrees well with results of alternate methods available in the literature.

## INTRODUCTION

There are two main groups of hybrid methods commonly used to derive acoustic sources from a CFD flow field and predict the propagation of these acoustic sources to the far field. An excellent review of these methods can be found in [1]. Methods in the first group are based on Lighthill's acoustic analogy [2, 3] and solve the CFD and sound propagation in a decoupled manner. The acoustic sources are extracted from the transient flow field data and then a wave equation, derived from Lighthill's acoustic analogy [2, 3], is solved to predict the propagation of these acoustic sources. Lighthill's acoustic analogy has been extended by several authors, most notably by Curle [4], Ffowcs Williams and Hawkings [5] and di Franciscantonio [6]. Curle [4] extended Lighthill's acoustic analogy to include the effect of stationary, impermeable rigid surfaces on the acoustic propagation. The work of Ffowcs Williams and Hawkings [5] allowed for the impermeable rigid surfaces to be in arbitrary motion and di Franciscantonio [6] further extended this to allow the surfaces to be permeable. Methods in the second group are based on the hydrodynamic/acoustic splitting of the solution variables. This leads to two sets of equations to be solved. One set of equations resolves the unsteady baseline hydrodynamic flow field while the other set of equations resolves the acoustic perturbations of the solution variables around this baseline flow. Using this approach the hydrodynamic and acoustic equations are solved in a coupled manner. Methods that fall into this second group include the expansion about incompressible flow (EIF) method of Hardin and Pope [7], the acoustic perturbation equation method of Ewert and Schröder [8], the perturbed compressible equations (PCE) and the linearised perturbed compressible equations (LPCE) methods of Seo and Moon [9, 10].

In the EIF method, the compressible Navier-Stokes equation is split such that the hydrodynamic solution is obtained by solving the incompressible Navier-Stokes equation and the acoustic solution is achieved by solving the perturbed Euler equation. Seo and Moon [9] demonstrate that excessive 'perturbed vorticity' is generated near wall boundaries in the EIF method due to coupling between the incompressible flow variables and the perturbed quantities. This leads to significant inaccuracies in the acoustic solution when using the EIF method for low Mach number flows [9]. Seo and Moon derived the PCE to more accurately represent the near field coupling phenomena responsible for the generation of this perturbed vorticity [9]. The amount of perturbed vorticity generated at solid boundaries with the PCE method is significantly less than that created with the EIF method. Despite this improvement, the perturbed vorticity generated by the PCE method still becomes easily unstable and causes inconsistent, grid dependent acoustic solutions [10]. Further investigations revealed that the effect of perturbed vorticity on sound generation is negligible at low Mach numbers [10]. Hence Seo and Moon developed the LPCE, a modified version of the PCE in which the generation of perturbed vorticity is suppressed [10]. One of the features of the LPCE is that the only acoustic source term is the material derivative of the hydrodynamic pressure.

The LPCE method has been shown to accurately predict the sound pressure field radiated from laminar flow [10] and turbulent flow [11] past a cylinder. One deficiency of the LPCE method in its present form is that it does not permit the influence of a flexible structure on the acoustic propagation to be calculated. Such fluid/structure interactions are very important in predicting sound fields radiated from marine vessels. In the present work a method has been developed

that extracts acoustic sources from an incompressible CFD simulation based on the LPCE source terms. The propagation of these acoustic sources is calculated using a BEM solver. The BEM solver that is used in the present method also contains a finite element method (FEM) solver that is able to simulate the vibro-acoustic response of structures. Coupling together these BEM and FEM solvers allows the effect of fluid/structure interaction on the acoustic propagation to be determined. Hence the method developed in this work can be extended to consider the interaction of flow-induced noise with a flexible marine vessel and the resulting far field sound radiation. The method presented here is similar to the decoupled approach of Lighthill [2, 3]. However, in the present method calculation of the acoustic source term requires the evaluation of a scalar quantity at each CFD cell, compared with Lighthill's approach which requires a tensor, Lighthill's Tensor, to be evaluated. Hence extracting acoustic source terms using the present approach will be more efficient than using Lighthill's analogy.

The aim of this work is to extract the acoustic sources generated by low Mach number flow past a cylinder and to predict the radiated sound pressure. This new hybrid CFD/BEM method is applied to predict the far-field acoustic pressure induced by the laminar flow past a cylinder at a Reynolds number,  $Re_D=100$  and Mach number,  $M=0.15$ . The successful outcomes of this work will have application to marine vessels, in order to predict the excitation of a ship or submarine hull due to pressure fluctuations from the propeller.

## NUMERICAL METHODS

### Linearised Perturbed Compressibility Equations

In the LPCE method, the total flow variables are decomposed into incompressible and perturbed components:

$$\begin{aligned}\rho &= \rho_0 + \rho' \\ \mathbf{u} &= \mathbf{U} + \mathbf{u}' \\ p &= P + p'\end{aligned}\quad (1)$$

where  $\rho$  is the total fluid density,  $\rho_0$  is the density of the incompressible fluid and  $\rho'$  is the density perturbation. Similarly  $\mathbf{u}$  is the total velocity vector of the fluid, where  $\mathbf{U}$  and  $\mathbf{u}'$  are respectively the incompressible and perturbed velocity vectors, and  $p$  is the total static pressure of the fluid, with  $P$  and  $p'$  representing the incompressible and perturbed components of static pressure, respectively. The LPCE are:

$$\frac{\partial \rho'}{\partial t} + (\mathbf{U} \cdot \nabla) \rho' + \rho_0 (\nabla \cdot \mathbf{u}') = 0 \quad (2)$$

$$\frac{\partial \mathbf{u}'}{\partial t} + \nabla(\mathbf{u}' \cdot \mathbf{U}) + \frac{1}{\rho_0} \nabla p' = 0 \quad (3)$$

$$\frac{\partial p'}{\partial t} + (\mathbf{U} \cdot \nabla) p' + \gamma P (\nabla \cdot \mathbf{u}') + (\mathbf{u}' \cdot \nabla) P = -\frac{DP}{Dt} \quad (4)$$

where  $\gamma$  is the ratio of specific heats. The term on the right hand side of equation (4) is the material derivative of the hydrodynamic pressure, given by:

$$\frac{DP}{Dt} = \frac{\partial P}{\partial t} + \mathbf{U} \cdot \nabla P \quad (5)$$

and is the only acoustic source term in the LPCEs. Equation (2) is the linearised continuity equation, with equations (3) and (4) representing the linearised conservation of momentum and conservation of energy equations, respectively. Seo

and Moon [9] derived a wave equation for the Perturbed Compressible Equations (PCE) method. Using this wave equation as a starting point, a wave equation for the LPCE is:

$$\begin{aligned}\nabla^2 p' - \frac{1}{c_0^2} \frac{\partial^2 p'}{\partial t^2} - \frac{1}{c_0^2} (\mathbf{U} \cdot \nabla) \frac{\partial p'}{\partial t} - \frac{1}{c_0^2} \left( \frac{\partial \mathbf{U}}{\partial t} \cdot \nabla \right) p' \\ - \frac{1}{c_0^2} \left( \frac{\partial \mathbf{u}'}{\partial t} \cdot \nabla \right) P - \frac{1}{c_0^2} (\mathbf{u}' \cdot \nabla) \frac{\partial P}{\partial t} - \frac{\gamma}{c_0^2} \frac{\partial P}{\partial t} (\nabla \cdot \mathbf{u}') \\ + \rho_0 \nabla \cdot \nabla(\mathbf{u}' \cdot \mathbf{U}) = \frac{1}{c_0^2} \frac{\partial}{\partial t} \left( \frac{DP}{Dt} \right)\end{aligned}\quad (6)$$

where the relationship  $\gamma P = \rho_0 c^2$  has been used in equation (4).

### Linear Wave Equation

In the presence of mean flow, the standard linear wave equation is obtained from the linearised continuity and momentum equations to give:

$$\begin{aligned}\nabla^2 p' - \frac{1}{c_0^2} \frac{\partial^2 p'}{\partial t^2} - \frac{1}{c_0^2} (\mathbf{U} \cdot \nabla) \frac{\partial p'}{\partial t} - \frac{1}{c_0^2} \left( \frac{\partial \mathbf{U}}{\partial t} \cdot \nabla \right) p' \\ + \rho_0 \nabla \cdot \nabla(\mathbf{u}' \cdot \mathbf{U}) = 0\end{aligned}\quad (7)$$

It is the similarity between equations (6) and (7) which has inspired the work contained herein. Using the equality of equation (7) in equation (6) the LPCE wave equation has the following additional terms relative to the linear wave equation:

$$\begin{aligned}- \frac{1}{c_0^2} \left( \frac{\partial \mathbf{u}'}{\partial t} \cdot \nabla \right) P - \frac{1}{c_0^2} (\mathbf{u}' \cdot \nabla) \frac{\partial P}{\partial t} - \frac{\gamma}{c_0^2} \frac{\partial P}{\partial t} (\nabla \cdot \mathbf{u}') \\ = \frac{1}{c_0^2} \frac{\partial}{\partial t} \left( \frac{DP}{Dt} \right)\end{aligned}\quad (8)$$

The term on the right hand side corresponding to  $\frac{1}{c_0^2} \frac{\partial}{\partial t} \left( \frac{DP}{Dt} \right)$  is the acoustic source term from the LPCE and will be extracted from an incompressible CFD simulation. The terms on the left hand side combine both perturbed and hydrodynamic variables and they will not be included in the approach presented here. These terms are acoustic scattering terms relating to the mean flow having a refraction effect which is negligible at low Mach numbers. Seo and Moon [10] examine the Mach number dependence of the terms in the wave equation they formulate for the PCEs. The terms that are set to zero in the current method are shown to be  $O(M^3)$ , whereas the leading order retained terms, including the acoustic source, are  $O(M)$  [10]. It is interesting to note that equation (8) is another equation that could be solved to predict the propagation of the acoustic source, although this will not be considered in the present work.

### Transient Laminar CFD Simulation

Laminar vortex shedding from a cylinder of diameter  $D$  is simulated at  $Re_D=100$  and  $M=0.15$ . For this simulation a two-dimensional circular domain around the cylinder has been modelled and analysed using ESI Group's CFD-ACE+ software package [12]. The Navier-Stokes equations are solved by CFD-ACE+ and in this instance a direct numerical simulation (DNS) of the flow field has been performed. In a 'sponge' region adjacent to the external boundaries of the computational domain, the viscosity has been artificially increased to damp out the fluctuations in the velocity field. A convective boundary condition was also applied to the outlet

boundary to prevent reflection of vorticity back into the computational domain. The convective boundary condition, based on the Sommerfield radiation condition, was first proposed by Orlanski [13] and has been successfully applied to transient CFD simulations involving vortex shedding [14, 15]. This boundary condition takes the form:

$$\frac{\partial u_i}{\partial t} + U_{conv} \frac{\partial u_i}{\partial n} = 0 \quad (9)$$

where  $U_{conv}$  is the convection velocity normal to the boundary and  $\frac{\partial u_i}{\partial n}$  represents the gradient of the  $i^{\text{th}}$  component of velocity normal to the outlet boundary.

The model used for the CFD simulation is shown in Figure 1, with the mesh topology in the vicinity of the cylinder inset. The interior of the computational domain extends radially for  $25D$ . The sponge layer extends radially for an additional  $20D$ . The interior domain contains 50,546 quadrilateral cells, with a cell spacing adjacent to the cylinder of  $0.0125D$ . The cell distribution is biased so that the wake region contains a high cell density to resolve the vortices shed from the cylinder. The sponge layer contains an additional 4,318 quadrilateral cells.

A steady state simulation was performed with the converged solution used as the initial condition of the transient simulation. The simulations were second order accurate in time and space, with a central difference scheme used for the spatial discretisation and a Crank-Nicholson scheme used for the temporal discretisation. The transient simulation was executed for 50,000 time steps with the time step size given by  $0.0476tU/D$ . This is equivalent to a time step of  $4.76E-4s$  and corresponds to a Courant-Friedrichs-Lewy (CFL) number of 3.8. This time step size is sufficient to capture approximately 500 vortex shedding periods. The simulation was allowed to progress until the flow field achieved periodicity. Recording of the acoustic source data commenced after this periodicity had been attained.

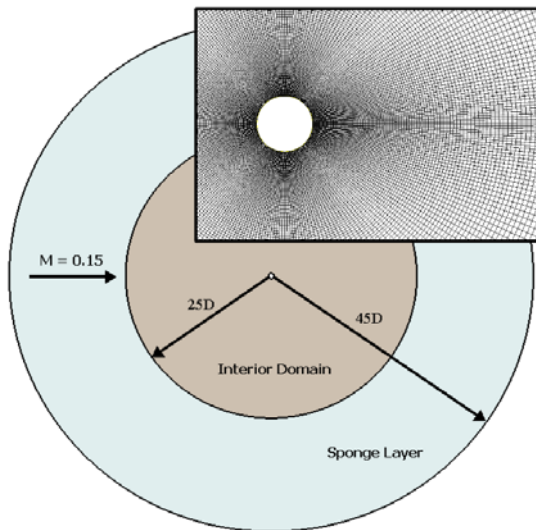


Figure 1. Domain shape and size for CFD analysis

### Boundary Element Method

The Boundary Element solver in ESI Group's vibro-acoustic simulation package, VA One 2010, is used to solve the acoustic propagation [16]. This boundary element method solves the harmonic wave (Helmholtz) equation and is able to

consider the effects of uniform mean flow on sound propagation.

For a uniform flow velocity  $\mathbf{U}=(U_x, 0, 0)$ , the Helmholtz equation can be expressed as:

$$\nabla^2 p' + k^2 p' - 2ikM \frac{\partial p'}{\partial x} - M^2 \frac{\partial^2 p'}{\partial x^2} = f \quad (10)$$

where  $f$  is an acoustic source,  $k(=\omega/c)$  is the wave number,  $\omega$  is the harmonic frequency and  $M=U_x/c_0$  is the Mach number. The boundary element model is driven by acoustic monopoles which are derived from the acoustic sources extracted from the transient CFD data. At each time step the acoustic source term generated in each CFD cell is given by:

$$S_n^i = \frac{1}{c_0^2} \frac{\partial}{\partial t} \left( \frac{DP_n^i}{Dt} \right) \quad (11)$$

where  $S_n^i$  is the acoustic source density of the  $i^{\text{th}}$  CFD cell at time step  $n$ , with units of  $\text{Pa}\cdot\text{m}^{-2}$ . This results in a time history of the acoustic source density for each CFD cell. The approach that has been adopted in the present work is to create an acoustic monopole at the centre of each CFD cell and use the acoustic source density to derive the complex frequency spectrum that defines each monopole.

In VA One 2010, an expression to determine the RMS pressure caused by an acoustic monopole source is given by:

$$P_{rms}(r, \omega) = \frac{|A(\omega)|}{4\pi r} \quad (12)$$

where  $|A(\omega)|$  is the modulus of the complex spectrum that defines the monopole and has units  $\text{Pa}\cdot\text{m}$ . It is important to note that the monopole is a point source, whereas  $S_n^i$  represents the acoustic source strength per unit volume. Hence the acoustic source density extracted from the CFD results must be multiplied by the CFD cell volume to give the total acoustic source acting at the cell centre:

$$R_n^i = S_n^i V^i \quad (13)$$

where  $R_n^i$  is the total acoustic source acting at the centre of the  $i^{\text{th}}$  cell at time step  $n$  and  $V^i$  is the volume of the  $i^{\text{th}}$  cell.

### Digital Signal Processing of Acoustic Source Data

To convert the acoustic source time histories into frequency spectra, a discrete Fourier transform (DFT) must be performed. The DFT assumes that the finite length time history is one period of an infinitely long periodic signal which requires  $R_0^i = R_N^i$ , where  $N$  is the final time step of the simulation. If this condition is not met, 'spectral leakage' occurs which pollutes the frequency spectra. For laminar vortex shedding from a cylinder it is relatively straight forward to specify a total simulation time that is an integer multiple of the vortex shedding period, thus ensuring that  $R_0^i = R_N^i$ . However the method developed herein will ultimately be applied to wall-bounded turbulent flows. While it may be possible to capture the periodicity of the large scale structures in such a flow, the smaller scale turbulent fluctuations may

not exhibit any periodicity and hence a more robust approach based on Welch's modified periodogram method [17] is used.

The acoustic source time history of each CFD cell is divided into equal segments and multiplied by a Hanning window function to enforce periodicity of each segment. The frequency spectra of each segment are then computed using the *fourl* and *realft* fast Fourier transform (FFT) algorithms of Press et al. [18]. An implementation of Welch's modified periodogram method [17] is programmed in Fortran 95 and used to calculate average power and cross spectrum for each acoustic source, with the cross spectrum calculated relative to the spectrum at top-dead centre of the cylinder. The power and cross spectrum for each acoustic source is converted to a complex pressure spectrum which is used to define these acoustic monopole at each CFD cell centre.

## RESULTS AND DISCUSSION

### Hydrodynamic Results

Figure 2 shows a plot of the vorticity in the flow field at one instance in time. The vorticity generated at the cylinder surface is shed from the cylinder and travels downstream as vortex pairs. Figure 2 also shows that the vorticity contours are smooth, which demonstrates that the sponge layer and convective boundary condition are successful at preventing reflection of vorticity from the downstream boundary.

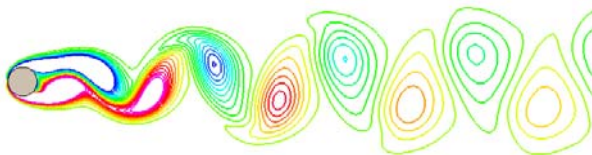


Figure 2. Vorticities in wake of cylinder

Figure 3 shows the frequency spectra of the fluctuating lift and drag forces exerted on the cylinder. The fundamental vortex shedding frequency is identified to be 16 Hz. This figure also illustrates that peaks of the fluctuating lift force occur at odd harmonics of the vortex shedding frequency and peaks of the drag force occur at even harmonics.

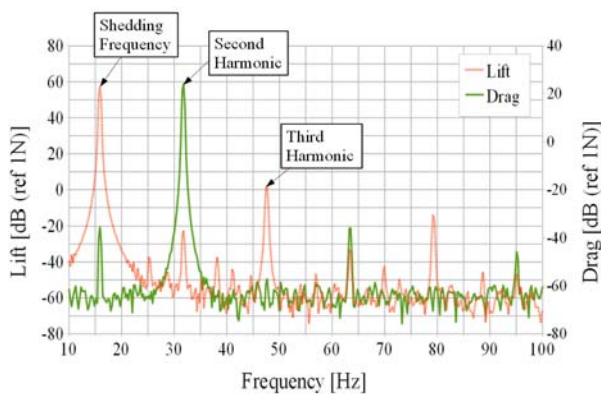


Figure 3. Frequency spectra of lift and drag forces

The mean drag coefficient calculated from the transient CFD simulation is  $C_D=1.29$  which compares well with the experimental value of 1.24-1.26 obtained by Tritton [19]. The Strouhal number predicted from the present analysis is  $St=0.16$ , which compares well with the experimental value of 0.164 reported by Fey et al. [20].

### Acoustic Source Extraction

Figure 4 shows the time evolution of the acoustic source density at four instances in time, with the range limited to -40 to 40 Pa.m<sup>2</sup> for clarity. Also, the source density plot at time step = 1 refers to the first time step after the CFD solution has attained periodicity, which has been assigned a time,  $t = 0.0$ s. Figure 4 shows that significant acoustic sources exist in the vicinity of the cylinder and in the wake of the cylinder.

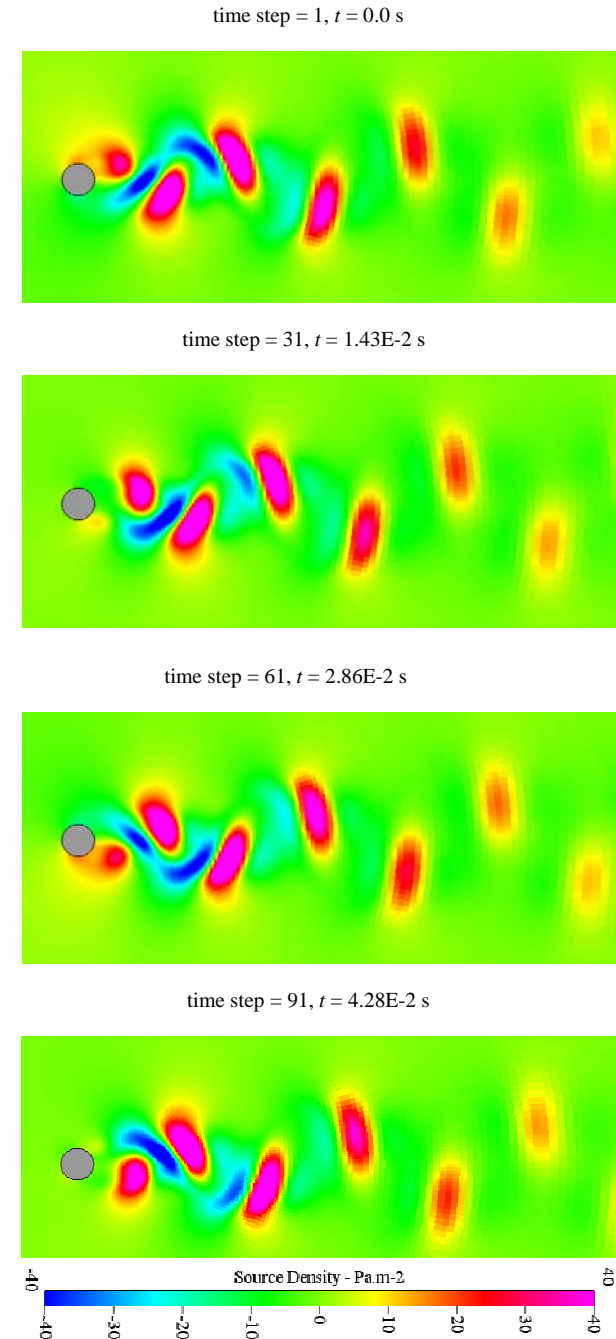
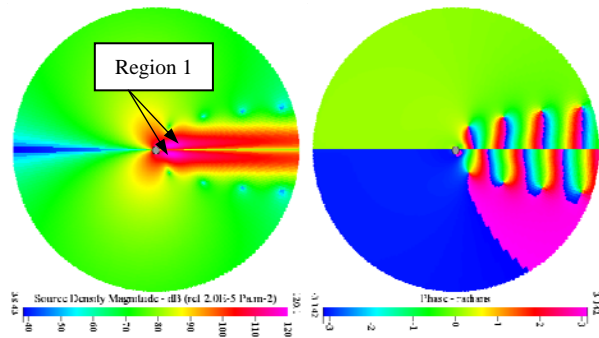


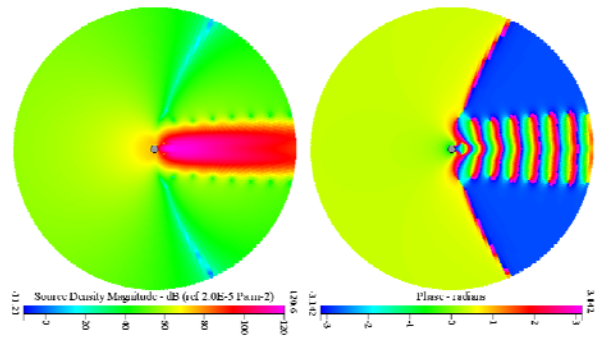
Figure 4. Time evolution of acoustic source density

Figure 5 shows the magnitude and phase of the acoustic source density extracted from the CFD results at the vortex shedding frequency and the second and third harmonics. The magnitude plots at the fundamental and third harmonic of the vortex shedding frequency demonstrate a strong symmetry along the cylinder centreline parallel to the flow direction. The phase plots at these frequencies show a trend that the monopole sources below the centreline are 180° out of phase with the monopole sources above the centreline. This is ex-

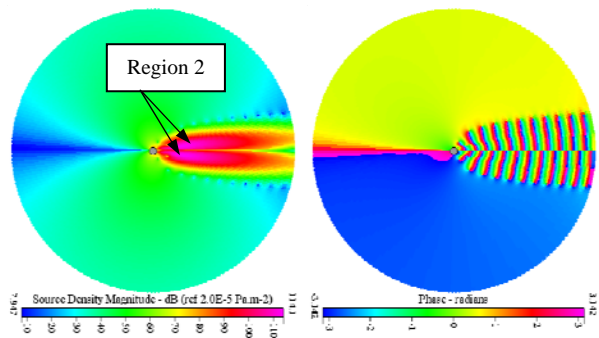
pected as the fundamental and third harmonic of the vortex shedding frequency coincides with peaks of the lift force spectra. The second harmonic of the vortex shedding frequency coincides with the first peak of the drag force spectra. The plot of source density magnitude at the second harmonic of the vortex shedding frequency again exhibits symmetry around the horizontal centerline. However the phase plot indicates that at this frequency, the acoustic sources on the front of the cylinder are  $180^\circ$  out of phase with those on the back of the cylinder. The region on the cylinder where this phase shift occurs is not at top and bottom dead centre as might be expected, rather the phase shift occurs in the region where the flow separates from the cylinder.



(a) Vortex shedding frequency



(b) Second harmonic of vortex shedding frequency



(c) Third harmonic of vortex shedding frequency

**Figure 5.** Magnitude and phase of acoustic source density

From Figure 5(a) and (c), regions 1 and 2 highlight areas in the cylinder wake where the acoustic sources are caused by vortex pairings shed from the cylinder. These vortex pairings result in acoustic sources at the fundamental and third harmonic of the vortex shedding frequency that are equal in magnitude and opposite in phase. This results in ‘monopole-monopole cancellation’ in the wake region of the cylinder. In the vicinity of the cylinder, this monopole-monopole cancellation is expected to produce pairs of dipole sources aligned

vertically, while further downstream the monopole-monopole cancellation will result in a distribution of quadrupole sources. These comments are in line with the findings of Lighthill [2, 3] and Curle [4]. Dipole sources radiate sound more efficiently than quadrupole sources and hence the directivity of the far-field sound pressure should resemble a dipole pattern at the fundamental and third harmonic of the vortex shedding frequency. Figure 5(b) shows significantly different distributions of magnitude and phase for the monopole sources at the second harmonic of the shedding frequency. At this frequency, the monopole-monopole cancellation is expected to produce pairs of dipole sources aligned horizontally. This is expected to result in the directivity of the far-field sound pressure resembling a dipole pattern aligned front-to-back relative to the cylinder, however this requires further investigation.

To display the acoustic source results shown in Figures 4 and 5, one discrete point was created for each monopole source and the results were visualised on these points. Using this approach, each point is displayed as a constant value, with no interpolation between adjacent points. Close to the cylinder, where the point density is highest, the results appear smooth. However, further away from the cylinder the point density decreases and the results appear more pixelated. This effect is most evident in Figure 4. For future work, an alternate method of visualising the acoustic source data will be used that will alleviate this problem.

**Far-Field Acoustics**

The directivity plot of the sound pressure field at the vortex shedding frequency is given in Figure 6. This directivity plot is compared with that presented by Khalighi et al. [21]. The data recovery points are placed on a circle of radius  $12.9 D$  centred at  $1.86 D$  downstream of the cylinder, which coincides with the front of a propagating and convecting sound wave that is generated at the cylinder [21]. The pressure is normalised by the peak RMS sound pressure recorded at the data recovery points. Figure 6 shows that the directivity of the sound pressure field predicted by the present method compares well with the results of Khalighi et al. [21].

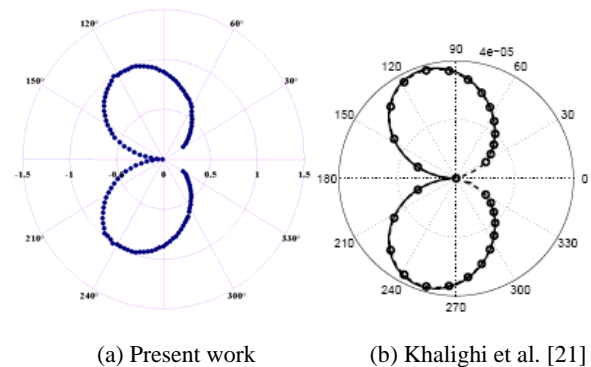


**Figure 6.** Directivity plot of sound pressure field at vortex shedding frequency

**CONCLUSIONS**

A hybrid CFD-BEM approach has been proposed to predict low Mach number flow induced noise. The method extracts acoustic sources from incompressible CFD data based on the LPCE source terms and then predicts the far field acoustic pressure by solving the harmonic wave equation using a BEM solver.

Visualisation of the time evolution of the acoustic source clearly shows acoustic source generation both in the vicinity of the cylinder as well as in the wake. Acoustic monopoles were created from the time histories of the acoustic source density extracted from the CFD simulation using Welch's modified periodogram method [17]. Plots of the magnitude and relative phase of these monopole sources suggest that the acoustic sources in the wake of the cylinder may form self-cancelling regions at the fundamental and third harmonic of the vortex shedding frequency that will limit the amount of sound pressure propagated downstream at these frequencies. The magnitude and phase plots also suggest that the fundamental and third harmonic of the vortex shedding frequency correspond to the first and second peaks of the lift force spectra respectively. Furthermore, the second harmonic of the vortex shedding frequency corresponds to the first peak of the drag force spectra. The directivity plot at the shedding frequency indicates that the sound pressure field at that frequency qualitatively matches the expected profile. Further work is underway to predict the directivity of the sound pressure field at the higher harmonics of the vortex shedding frequency.

### ACKNOWLEDGEMENTS

Funding for this work has been provided by the Maritime Platforms Division of the Defence Science and Technology Organisation. Financial assistance from the Australian Acoustical Society (NSW Division) for a *Young Scientist's Award* to participate at the ICA2010 conference is gratefully acknowledged.

### REFERENCES

- 1 C. Cheong, P. Joseph, Y. Park and S. Lee, "Computation of aeolian tone from a circular cylinder using source model", *Applied Acoustics*, **69**, 110–126 (2008)
- 2 M.J. Lighthill, "On sound generated aerodynamically, I. general theory", *Proceedings of the Royal Society A*, **211**, 564–587 (1952)
- 3 M.J. Lighthill, "On sound generated aerodynamically, II. Turbulence as a source of sound", *Proceedings of the Royal Society A*, **222**, 1–32 (1954)
- 4 N. Curle "The influence of solid boundaries upon aerodynamic sound", *Proceedings of the Royal Society of London A*, **231**, 505–514 (1955)
- 5 J.E. Ffowcs Williams and D.L. Hawkings, "Sound generation by turbulence and surfaces in arbitrary motion", *Philosophical Transactions of the Royal Society Series A*, **264**, 321–342 (1969)
- 6 P. di Franciscantonio, "A new boundary integral formulation for the prediction of sound radiation", *Journal of Sound and Vibration*, **202**, 491–509 (1997)
- 7 J.C. Hardin and D.S. Pope, "An acoustic/viscous splitting technique for computational aeroacoustics", *Theoretical and Computational Fluid Dynamics*, **6**, 323–340 (1994)
- 8 R. Ewert and W. Schröder, "Acoustic perturbation equations based on flow decomposition via source filtering", *Journal of Computational Physics*, **188**, 365–398 (2003)
- 9 J.H. Seo and Y.J. Moon, "Perturbed compressible equations for aeroacoustic noise prediction at low Mach numbers", *AIAA Journal*, **43**, 1716–1724 (2005)
- 10 J.H. Seo and Y.J. Moon, "Linearized perturbed compressible equations for low Mach number aeroacoustics", *Journal of Computational Physics*, **218**, 702–719 (2006)
- 11 J.H. Seo and Y.J. Moon, "Aerodynamic noise prediction for long-span bodies", *Journal of Sound and Vibration*, **306**, 564–579 (2007)
- 12 *CFD-ACE+ V2009.4 User Manual*, ESI Group, Paris, France 2009
- 13 I. Orlanski, "A simple boundary condition for unbounded hyperbolic flows", *Journal of Computational Physics*, **21**, 251–269 (1976)
- 14 M. Breuer, "Numerical and modeling influences on large eddy simulations for the flow past a circular cylinder", *International Journal of Heat and Fluid Flow*, **19**, 512–521 (1998)
- 15 M. Breuer, "A challenging test case for large eddy simulation: high Reynolds number circular cylinder flow", *International Journal of Heat and Fluid Flow*, **21**, 648–654 (2000)
- 16 *VA One 2010 User's Guide*, ESI Group, Paris, France, June 2010
- 17 P.D. Welch, "The use of fast Fourier transform for the estimation of power spectra: a method based on time averaging over short, modified periodograms", *IEEE Transactions on Audio Electroacoustics*, **15**, 70–73 (1967)
- 18 W.H. Press, S.A. Teukolsky, W.T. Vetterling, and B.P. Flannery", *Numerical Recipes in Fortran (The Art of Scientific Computing)*, Cambridge University Press, Cambridge, 2<sup>nd</sup> edition, 1992
- 19 D.J. Tritton, "Experiments on the flow past a circular cylinder at low Reynolds numbers", *Journal of Fluid Mechanics*, **6**, 547–567 (1959)
- 20 U. Fey, M. König, and H. Eckelmann, "A new Strouhal–Reynolds-number relationship for the circular cylinder in the range  $47 < Re < 2 \times 10^5$ ", *Physics of Fluids*, **10**, 1547–1549 (1998)
- 21 Y. Khalighi, A. Mani, F. Ham, and P. Moin "Prediction of sound generated by complex flows at low Mach numbers", *AIAA Journal*, **48**, 306–316 (2010)